Marky, L. A., & Breslauer, K. J. (1987) *Proc. Natl. Acad. Sci. U.S.A. 84*, 4359–4363.
Marky, L. A., Blumenfeld, K. S., & Breslauer, K. J. (1983) *Nucleic Acids Res. 11*, 2857–2870.
Martin, R. F., & Holmes, N. (1983) *Nature 302*, 452–454.
McGhee, J. D., & von Hippel, P. H. (1974) *J. Mol. Biol. 86*, 469–489.
Mikhailov, M. V., Zasedatelev, A. S., Krylov, A. S., & Gurskii, G. V. (1981) *Mol. Biol. (Moscow) 15*, 541–554.
Pjura, P. E., Grzeskowiak, K., & Dickerson, R. E. (1987) *J. Mol. Biol. 197*, 257–271.
Portugal, J., & Waring, M. J. (1988) *Biochim. Biophys. Acta 949*, 148–158.
Pullmann, B. (1985) *Proc. Int. Symp. Biomol. Struct. Interact., Suppl. J. Biosci. 8*, 681–688.
Record, M. T., Lohman, T. M., & DeHaseth, P. (1976) *J. Mol. Biol. 107*, 145–158.
Record, M. T., Anderson, C. F., & Lohman, T. M. (1978) *Q. Rev. Biophys. 11*, 103–178.
Regenfuss, P., Loontiens, F. G., & Clegg, R. M. (1989) *Arch. Int. Physiol. Biochem. 97*, B113.
Scheibe, G. (1939) *Angew. Chem. 52*, 631–637.
Schellman, J. A. (1974) *Isr. J. Chem. 12*, 219–238.
Simon, R. H., & Felsenfeld, G. (1979) *Nucleic Acids. Res. 6*, 689–696.
Steiner, R. F., & Sternberg, H. (1979) *Arch. Biochem. Biophys. 197*, 580–588.
Stokke, T., & Steen, H. B. (1985) *J. Histochem. Cytochem. 33*, 333–338.
Teng, M.-K., Usman, N., Frederick, C. A., & Wang, A. H.-J. (1988) *Nucleic Acids Res. 16*, 2671–2690.
Weisblum, B., & Haenssler, E. (1974) *Chromosoma 46*, 255–260.
Yuzhakov, V. I. (1975) *Russ. Chem. Rev. 48*, 1076–1091.
Zasedatelev, A. S., Gurskii, G. V., & Volkenshtein, M. V. (1971) *Mol. Biol. 5*, 245–251.
Zimmer, C., & Waehnert, U. (1986) *Prog. Biophys. Mol. Biol. 47*, 31–112.

# Characterization of the Secondary Structure and Melting of a Self-Cleaved RNA Hammerhead Domain by $^1$H NMR Spectroscopy†

Ann Caviani Pease and David E. Wemmer*
*Department of Chemistry and Chemical Biodynamics Division, Lawrence Berkeley Laboratory, University of California, Berkeley, California 94720*

*Received February 9, 1990; Revised Manuscript Received June 26, 1990*

ABSTRACT: We have completely assigned the extreme low-field ring–NH nuclear magnetic resonance spectrum of a self-cleaving RNA in the absence of magnesium ions by experiments involving sequential Overhauser enhancements between adjacent base pairs. These assignments substantiate the hammerhead secondary folding model proposed by Symons and co-workers for this class of self-cleaving RNA [Hutchins, C. J., Rathjen, P. D., Forster, A. C., & Symons, R. H. (1986) *Nucleic Acids Res. 14*, 3627–3640; Forster, A. C. & Symons, R. H. (1987) *Cell 49*, 211–220; Kneese, P., & Symons, R. H. (1987) in *Viroids and Viroid-like Pathogens* (Semancick, J. S., Ed.) pp 1–47, CRC Press, Boca Raton, FL]. No resonances due to tertiary base pairs could be identified in the low-field spectrum, and addition of $MgCl_2$ to the sample did not produce additional resonances in this region of the spectrum.

A site-specific self-cleavage reaction has been observed for the (+) and (−) strands of satellite tobacco ringspot virus RNA (STobRV RNA) which results in 5′-hydroxyl and cyclic 2′,3′-phosphate termini (Prody et al., 1986; Buzayan et al., 1986a,b). Similar reactions have been observed for the (+) and (−) strands of avocado sunblotch virusoid (Hutchins et al., 1986) and lucerne transient streak viroid (Forster & Symons, 1987). Buzayan and co-workers have found that fewer than 100 nucleotides are necessary for efficient cleavage of (+) STobRV RNA (Buzayan et al., 1986). Symons and co-workers have proposed a hammerhead secondary folding model for the self-cleavage domain (Hutchins et al., 1986; Forster & Symons, 1987; Keese et al., 1987). This domain consists of 13 conserved nucleotides and 3 variable-length double-stranded helices (Figure 1). Cleavage occurs only at a specific phosphodiester linkage and requires no cofactor other than magnesium ions. Although the nucleotides directly at and near the cleavage site may vary, the position of cleavage within the hammerhead domain is conserved. Therefore, it is clear that a specific three-dimensional folding of the hammerhead domain is required for cleavage. The nature of the interactions giving rise to this folding is as yet unknown.

We have chosen to study the three-dimensional structure of such an RNA by nuclear magnetic resonance (NMR). NMR has been used extensively to study the structure of transfer RNA (tRNA) in solution. Particular attention has been paid to the extreme low-field (15–11 ppm) region of the spectrum [for reviews, see Kearns and Shulman (1974), Kearns (1976, 1977), Reid and Hurd (1977), Schimmel and Redfield (1980), and Reid (1981)]. Usually only hydrogen-bonded imino protons involved in secondary and tertiary base pairs resonate in this region, leaving it comparatively well resolved for a large nucleic acid (Reid et al., 1975, 1977, 1979). One-dimensional nuclear Overhauser enhancements (NOEs)

† This work was supported by the Office of Energy Research, Office of Health and Environmental Research, Health Effects Research Division of the U.S. Department of Energy, under Contract DE-AC03-76SF00098 and through instrumentation grants from the U.S. Department of Energy (DE FG05-86ER75281) and the National Science Foundation (DMB 86-09035 and BBS 87 20134).
* Address correspondence to this author at the Department of Chemistry, University of California, Berkeley.

0006-2960/90/0429-9039$02.50/0 

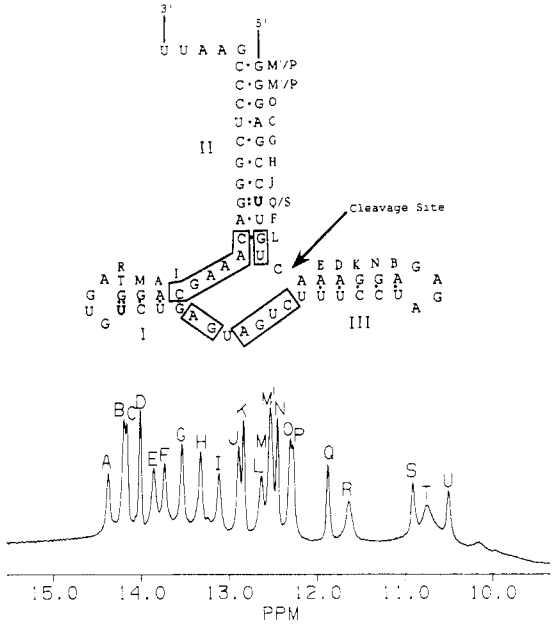


FIGURE 1: RNA sequence arranged in the hammerhead motif and the 500-MHz imino proton spectrum taken at 20 °C in 90% $H_2O$/10% $D_2O$, 20 mM phosphate buffer, pH 7, 0.1 M NaCl, 0.2 mM EDTA, and 0.02% $NaN_3$. The conserved nucleotides are boxed, the cleavage site is denoted by the arrow. Bases which are paired are connected with a dot. The assignments are discussed in the text.

have been used to assign this region of the spectrum for tRNA (Johnston & Redfield, 1978, 1981; Hare & Reid, 1982a,b), and the solution dynamics have been monitored under different solvent and temperature conditions (Reid, 1981). We have used this NOE methodology to assign the low-field spectrum of a self-cleaved RNA, and have studied the stability of helical regions with respect to temperature in the absence and presence of magnesium ions.

Figure 1 shows the RNA sequence we have designed with the conserved nucleotides boxed. The RNA is produced by in vitro T7 RNA polymerase run-off transcription, and because both this reaction and the cleavage reaction require magnesium ions, the RNA is cleaved at the site denoted by the arrow prior to purification. As an initial starting point, we have made the assumption that cleavage does not result in a significant rearrangement of the tertiary structure, and therefore this species approximates a true "cleavage conformation". Although this specific RNA sequence does not occur in nature, cleavage at the appropriate site has been demonstrated by showing that two RNA fragments of the correct sizes are formed, as analyzed by polyacrylamide gel electrophoresis (PAGE) under denaturing conditions (Figure 2). In particular, this sequence contains two GU wobble base pairs, one closing the hairpin loop of stem I, and the other within stem II, that are not present in any of the naturally occurring hammerhead-type self-cleaving RNAs. They were introduced to facilitate the NMR assignments. The logic behind the use of GU wobble pairs was 3-fold: (i) GU wobble pairs contain two hydrogen-bonded imino protons, allowing for two independent nearest-neighbor assignment pathways; (ii) the two imino protons of wobble pairs usually resonate slightly upfield of Watson–Crick-type imino protons, reducing chemical shift degeneracies; and (iii) the two imino protons produce strong (30–40%) mutual NOEs due to their close spatial proximity (<3 Å), which facilitates their assignment. In fact, GU4 of yeast $tRNA^{Phe}$ (Johnston & Redfield, 1978) and GU50 of *Escherichia coli* $tRNA^{fMet}$ (Hurd & Reid, 1979) and *E. coli* $tRNA_1^{Val}$ (Johnson & Redfield, 1979) were the first reliably assigned resonances in their respective low-field spectra (Reid, 1981). In addition, X-ray crystallographic studies of base pairing in DNA have shown that replacing a Watson–Crick GC pair with a GT wobble pair produces minimal perturbation in backbone torsion angles (Kneale et al., 1985; Ho et al., 1985).

## Materials and Methods

*RNA Samples.* Milligram quantities of RNA were produced by T7 RNA polymerase run-off transcription of a linear plasmid DNA template (Lowary et al., 1987). The proper RNA transcript was separated from plasmid DNA and short fall-off initiates on a 20 × 40 × 0.1 cm 12% polyacrylamide native slab gel. The RNA was visualized by shadowing with short-wave UV light on a fluorescent TLC plate. The band was excised from the gel and the RNA eluted by soaking the crushed gel slice in 0.1 M Tris·HCl, pH 7.5 at 37 °C, 15 mM EDTA, 0.15 M NaCl, and 1% (w/v) SDS at 37 °C for 24 h. The aqueous phase was carefully removed from the acrylamide pieces by using a drawn-out Pasteur pipet, and the RNA was precipitated for 4 h at −20 °C in 3 volumes of ethanol. After centrifugation at 15K rpm and 4 °C for 20 min, the pellet was dissolved in 2 mL of 5 mM potassium phosphate buffer, pH 7.0, and dialyzed for 24 h against 4 L of 5 mM potassium phosphate buffer, pH 7.0, 0.025 M NaCl, 0.05 mM EDTA, and 0.0005% $NaN_3$. After removal from the dialysis tubing, the RNA was dried by lyophilization and stored at −20 °C. A 20-mL transcription reaction containing 4 mg of linear plasmid DNA yielded 12 mg of pure RNA, representing a turnover of 400 copies of RNA per DNA template.

*Demonstration of Cleavage at the Appropriate Site.* Two micrograms of cleaved RNA and 2 μg of uncleaved RNA (α-S-A RNA) [transcribed as above replacing ATP with adenosine 5′-*O*-(1-thiotriphosphate)] were dissolved in 5 μL of denaturing loading buffer (90% deionized formamide, 0.05% bromophenol blue, and 0.05% xylene cyanol-FF) and heated for 1 min at 90 °C. Three microliters from each sample was immediately loaded onto an 8 × 10 × 0.07 cm 20% polyacrylamide gel containing 7 M urea. Electrophoresis was carried out against 1× TBE buffer (0.089 M Tris·borate, 0.089 M boric acid, and 2 mM EDTA) at 25-W constant power for 1 h. The gel was stained with 0.02% (w/v) toluidine blue-O (Sigma) for 2 min, destained with water for approximately 4 h, and photographed.

The large cleavage fragment (LF) was isolated from an 8 × 10 × 0.07 cm 20% polyacrylamide gel containing 7 M urea as previously described; 0.02 μg of LF was 5′-$^{32}$P end-labeled in a 20-μL reaction containing 50 mM Tris·HCl, pH 7.6 at 37 °C, 10 mM $MgCl_2$, 5 mM DTT, 0.1 mM spermidine, 0.1 mM EDTA, 2 μM ATP, 1 μL of [γ-$^{32}$P]ATP (Amersham, >5000 Ci/mmol, 10 mCi/mL), and 10 units of T4 polynucleotide kinase (BRL) (Maniatis et al. 1982, pp 122–124); 0.2 μg of a polythymidine ladder [poly(dT)] was similarly end-labeled. After incubation for 1 h at 37 °C, the reactions were quenched by addition of 2 μl of 0.5 M EDTA, the kinase was removed by extraction with 50:50 phenol/chloroform, and the nucleic acids were precipitated with ethanol. The pellets were dissolved in 20 μL of TE buffer; 2 μL of the RNA solution was added to a tube containing 2 μL of 10 mM $Pb(OAc)_2$, and this mixture incubated at 37 °C for 1 h to generate a sequence ladder. The poly(dT) was similarly dispensed into a tube containing 2 μL of TE buffer; 4 μL of 10 mM EDTA and 2 μL of 6X gel loading buffer (30% glycerol, 0.25% bromophenol blue, and 0.25% xylene cyanol-FF) were added to each tube. The nucleic acids were denatured by heating to 90 °C for 1 min, the tubes were immediately placed in an

ice/water bath, and at various times, 2 μL of each sample was loaded onto a 20 × 40 × 0.04 cm 20% polyacrylamide gel containing 7 M urea. Electrophoresis was carried out against 1× TBE buffer at 25-W constant power for a total of 4 h. Between loadings, the tubes were kept on ice. The actual running time for each lane is indicated in the legend of Figure 2.

*NMR Spectra.* Twelve milligrams of pure, lyophilized RNA was dissolved in 0.5 mL of 90% $H_2O$/10% $D_2O$ to give 1 mM RNA, 20 mM potassium phosphate, 0.1 M NaCl, 0.2 mM EDTA, and 0.2% $NaN_3$ solution at pH 7. This was transferred directly to Wilmad 528pp NMR tube. Between NMR experiments, the solution was removed from the NMR tube and the RNA stored at −20 °C as a lyophilized powder. For spectra recorded in the presence of magnesium ions, $MgCl_2$ was added to 10 mM.

Melting were collected on a GN500 spectrometer using a 1-*3*-3-*1* pulse (Hore, 1983) with the carrier frequency set at the resonance of water. A total of 1024 scans of 8K data points with a recycle delay of 0.5 s were averaged for each temperature increment. The data were Fourier-transformed, phase-corrected, and base-line-corrected using a MicroVax III workstation and FTNMR software (D. Hare, unpublished experiments). The spectra are indirectly referenced through the chemical shift of water at each temperature.

A complete set of NOE experiments was collected at both 15 and 20 °C. For these experiments, a peak of interest was selectively saturated by using decoupler irradiation at that frequency. The decoupler power level was adjusted to saturate 90% of peak D in 0.8 s. If one of a nearly degenerate pair of peaks was to be saturated, the decoupler frequency was set slightly off the exact top of the resonance in the direction away from the adjacent neighbor to reduce irradiation spillover. The NOE data were collected as two experiments: one with the decoupler set on-resonance for a peak of interest and the other with the decoupler set-off-resonance. The two experiments were collected in parallel, switching between on- and off-resonance at every scan. A total of 1024 scans of 8K data points were averaged for each experiment. The off-resonance FID was subtracted from the on-resonance FID on the GN500 and the resultant FID transferred to a MicroVax workstation. Fourier transformation, phase-correction, and base line correction using FTNMR software (D. Hare, unpublished results) generated the difference spectra.

## Results

Figure 2A shows the photograph of the 20% denaturing PAGE minigel. In Figure 2A, the large (LF) and small (SF) cleavage fragments are labeled on the gel, as well as the positions of the xylene cyanol-FF (XC) and bromophenol blue (BPB) dye markers. Uncleaved, α-S-A RNA runs more slowly than the large fragment, indicative of a longer nucleotide sequence. In addition, both cleavage products have a mobility consistent with their respective length when compared to the mobility of the dye markers (Maniatis et al., 1982). In an effort to count the number of nucleotides of the cleavage products, a ladder of 5'-$^{32}$P end-labeled LF was generated (Figure 2A). The lengths of the poly(dT) molecular weight marker are denoted on the gel. According to Figure 1, the large fragment is 54 nucleotides in length. The poly(dT) ladder cannot be used for a direct length comparison as the RNA bands suffer from sequence-specific migration rates. It can, however, be used to help orient the LF bands when comparing different lanes. Using the poly(dT) lane in this fashion, it is possible to count 53–54 bands in the LF ladder. The discrepancy arises from the ambiguity of whether the

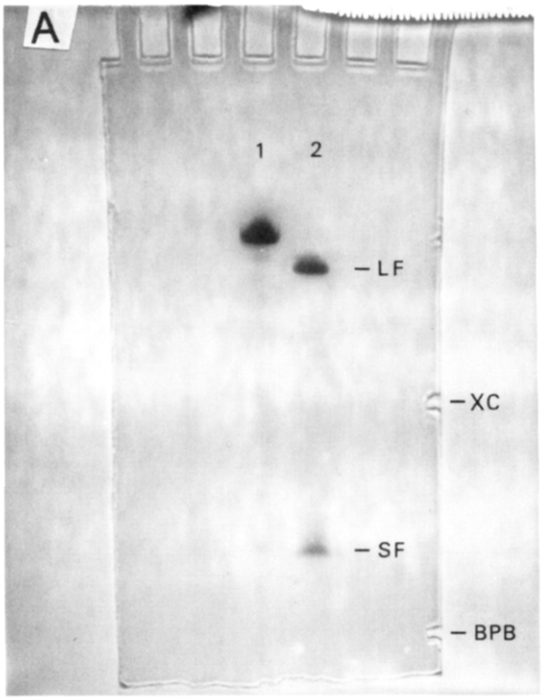


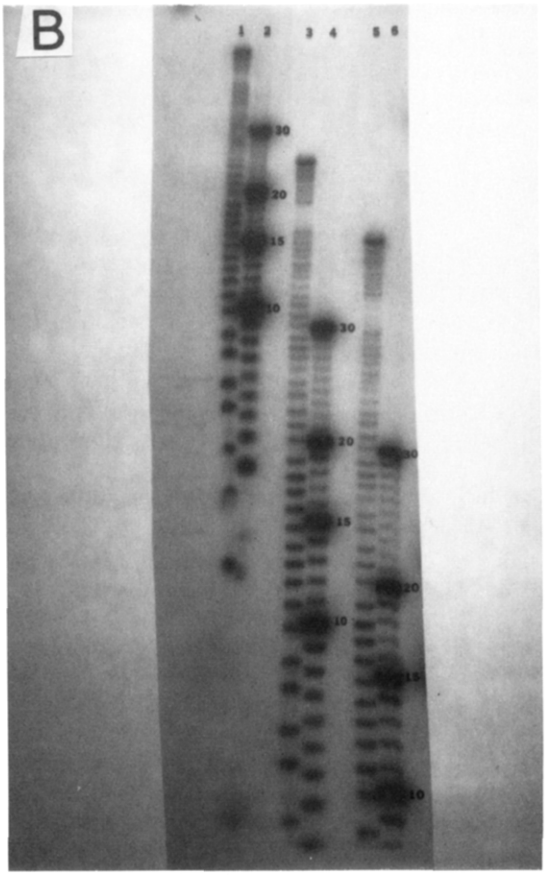


FIGURE 2: (A) 20% denaturing PAGE of RNA isolated from native gels. Lane 1, uncleaved α-S-A RNA; lane 2, cleaved RNA. The positions of the large (LF) and small (SF) cleavage products are denoted on the figure. The notches on the right side of the gel indicate the positions of the xylene cyanol-FF (XC) and bromophenol blue (BPB) dye markers and are labeled accordingly. (B) 20% denaturing PAGE of the ladder generated from 5'-$^{32}$P end-labeled LF. The lengths of the poly(dT) molecular weight marker bands are denoted on the figure in nucleotides. Lanes 1 and 2 ran for 1.25 h, lanes 3 and 4 ran for 2.5 h, and lanes 5 and 6 ran for 4.0 h.

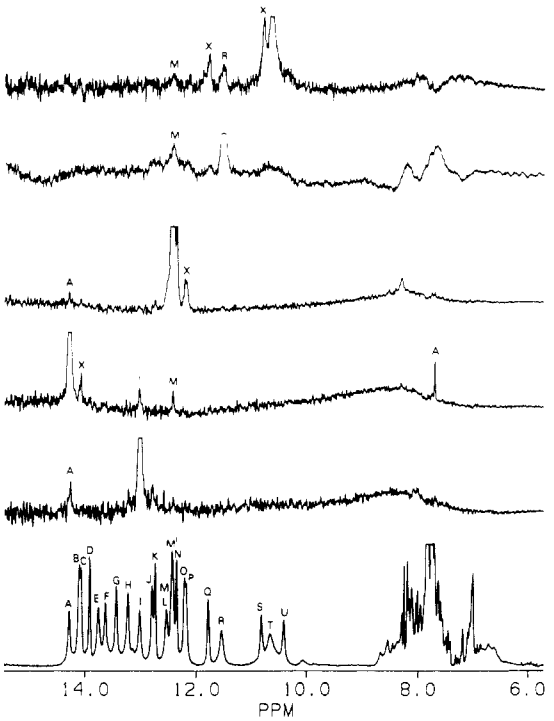


FIGURE 3: 500-MHz NOE difference spectra establishing the connectivities of stem I. The large, unlabeled resonances are the preirradiated peaks. NOEs are labeled in uppercase letters according to the reference spectrum. Peaks due to spill-over irradiation are labeled with an "X". Spectra corresponding to the saturation of resonances R and T were recorded at 15 °C, all others were recorded at 20 °C.

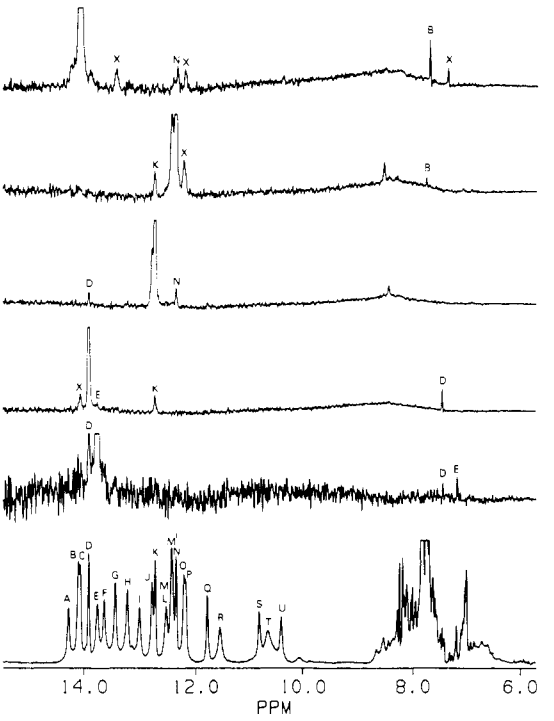


FIGURE 4: 500-MHz NOE difference spectra establishing the connectivities of stem III. The large, unlabeled resonances are the preirradiated peaks. NOEs are labeled in uppercase letters according to the reference spectrum. Peaks due to spill-over irradiation are labeled with an "X". All spectra were recorded at 20 °C.

lowest band on the gel corresponds to a single nucleotide or a dinucleotide. However, we feel that the evidence presented, namely, that cleaved RNA isolated from a native gel separates into two bands of the appropriate lengths on a denaturing gel, coupled with the ability to count a ladder generated from the isolated large fragment to within one nucleotide, and the fact that RNA prepared with adenosine 5′-*O*-(1-thiotriphosphate) cleaves slowly, indicating that the reactive site is to the 5′ side of an A residue, is overwhelming evidence that cleavage is occurring at the site denoted by the arrow in Figure 1. The fact that uncleaved $\alpha$-S-A RNA runs more slowly than the large cleavage fragment on a denaturing gel further supports this conclusion. Several attempts were made to similarly hydrolyze the small cleavage product with no success, as the small cleavage fragment degraded during handling.

The imino proton spectrum of our self-cleaving RNA has been completely assigned. The base pair type was determined from intra-base pair imino to aromatic C2H (Watson–Crick AU pairs) or amino proton (Watson–Crick GC pairs) NOEs (Sanchez et al. 1980), and inter-base pair imino–imino NOE determined nearest-neighbors (Johnston & Redfield, 1981). In cases where near-degeneracies in chemical shift occurred, second-order NOEs, representing next-nearest-neighbor connectivities, were used to aid the assignment procedure.

Figure 3 shows the imino–imino NOEs which establish the sequential connectivity of peaks R/T-M-A-I. Irradiation of resonance T, which is broad even at 15 °C, produces a strong NOE to R and a weak NOE to M. This NOE pattern is indicative of a GU wobble pair, and because both R and T have only one nearest-neighbor NOE to M, this GU wobble must be a terminal base pair. The only terminal GU wobble is that which closes the hairpin loop of stem I (Figure 1), and therefore the sequential connectivity R/T-M-A-I must define stem I. This assignment is corroborated by the NOEs of peaks A and I. Irradiation of resonance A produces a strong NOE to an aromatic C2H at 7.8 ppm, indicating that it is an AU base pair, and weaker sequential NOEs to I and M. Irradiation of resonance I produces the expected NOE to A and no others, identifying it as a terminal base pair.

Figure 4 shows the imino–imino NOEs sequentially connecting resonances E-D-K-N-B. The near-degeneracy of resonances B and C and the lack of NOE to B upon irradiation of N make the N-B connectivity slightly ambiguous. However, two lines of evidence support this assignment. The first is that although irradiation of peak N does not result in a sequential NOE to B, it does not result in an NOE to the aromatic C2H associated with B. Second, as the temperature is increased to 30 °C, resonance B broadens and disappears. Irradiation of peak C at 30 °C results in NOEs only to peaks O and G (Figure 5), meaning that it must be saturation of resonance B which results in an NOE to resonance N. The imino–imino NOE connecting E and D is also weak, but again NOEs to a common aromatic C2H confirm this assignment. The sharp NOEs to aromatic C2H's identify resonances B, D, and E as AU base pairs. Because sequential AU pairs are unique to stem III (Figure 1), determination of the D–E connectivity assigns resonances E-D-K-N-B as those of stem III.

Figure 6 shows the imino–imino NOEs sequentially connecting the resonances of stem II. Saturation of P produces a spillover peak to N and an NOE to M′. Saturation of M′ results in the expected NOE back to P. Saturation of O produces NOEs to M′ and C. Due to the near chemical shift degeneracy of peaks O and P, it is impossible to determine if the actual connectivity is P-M′-O or M′-P-O. However, it is clear that resonance O and not P is connected to C, as saturation of P produces only a very weak NOE to C whereas that of O is much more intense. Saturation of C produces NOEs to peaks O and G, and in addition produces a sharp NOE to the aromatic region of the spectrum identifying it as being manifested from an AU base pair. Continuing in a similar

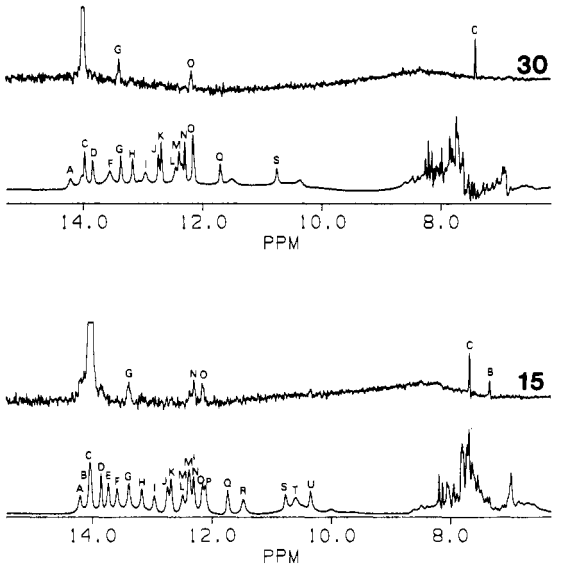


FIGURE 5: 500-MHz NOE difference spectra of nearly degenerate resonances B and C at 15 and 30 °C. Saturation of resonance B/C at 15 °C produces NOEs to G, N, and O, and two sharp aromatic NOEs. At 30 °C, saturation of B/C produces only one sharp aromatic NOE and imino NOEs to resonances G and O, proving that it is resonance B, and not C, which is the nearest neighbor of N.

manner, the connectivity can be contained through resonance J. Saturation of J produces three NOE to peaks H, Q, and S. In addition, Q and S produce strong NOEs, identifying these resonances as those of a GU wobble base pair. Saturation of F produces an NOE to L and a sharp aromatic NOE, identifying it as an AU base pair. However, at 20 °C, saturation of F does not produce NOEs to peaks Q and S as its assignment in Figure 1 requires. Nor does saturation of resonance L produce the expected NOE back to F. These connectivities were determined at 15 °C (Figure 7). Clearly, at this temperature, saturation of F produces NOEs to L, Q, and S in addition to its sharp aromatic NOE, and saturation of L produces a real, albeit weak, NOE to F. The fact that a GU wobble pair is connected to an AU and a GC pair identifies the M/P-M′/P-O-C-G-H-J-Q/S-F-L pathway as being that of stem II. This assignment is corroborated by the position of the two AU base pairs within the stem II sequence.

There is no NMR evidence to substantiate the existence of the AU base pairs terminating stems II and III proposed by the hammerhead model. In similar studies of two other hammerhead RNA sequences, no imino resonances corresponding to these base pairs were observed (data not shown). Irradiation of resonance U at both 20 and 15 °C produced no aromatic or imino NOEs (data not shown). It is most likely an imino proton in a hairpin loop or single-stranded region of the molecule which is somewhat protected from rapid exchange with $H_2O$. It is possible that this is from a tertiary interaction, but further data are needed to determine if this is in fact the case.

Figure 8 shows the imino region of the spectrum plotted as a function of temperature. An imino proton resonance will be observed only if the lifetime of the imino proton is long compared to the chemical shift difference between the imino form and the solvent. As the temperature is increased, base pairs begin to open, allowing the imino proton to exchange with $H_2O$. This is observed in NMR spectrum as a broadening, and eventual disappearance, of the imino resonance. Although the imino proton exchange rate is not limited by base pair opening (Leroy et al., 1985), the order of resonance broadening generally does follow the order of melting. When the helical stems are treated as individual subdomains of the hammerhead, the opening of individual base pairs can be monitored as each helical stem melts. The melting behavior was used to corroborate the NOE assignments by looking for apparent aberrant stability of base pairs.

On the basis of helical length, stem I should melt before stem II and probably simultaneously with stem III. As the

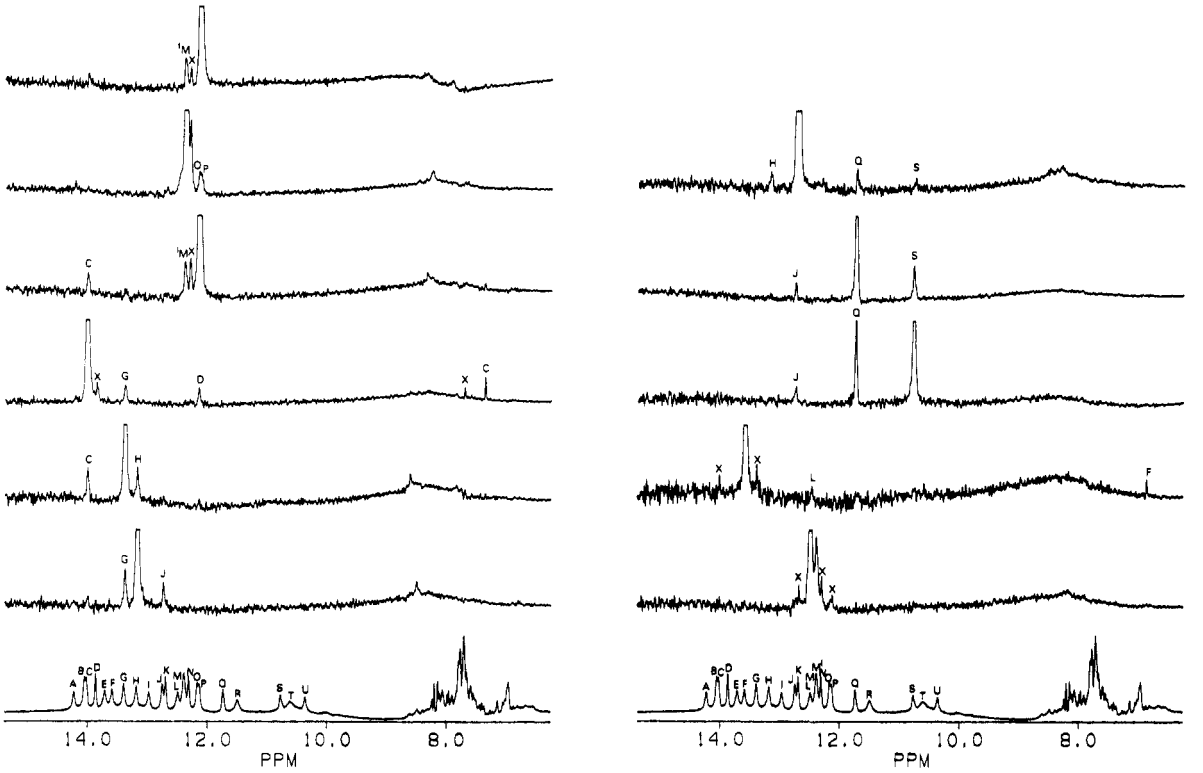


FIGURE 6: 500-MHz NOE difference spectra establishing the connectivities of stem II. The large, unlabeled resonances are the preirradiated peaks. NOEs are labeled in uppercase letters according to the reference spectrum. Peaks due to spill-over irradiation are labeled with an "X". All spectra were recorded at 20 °C.

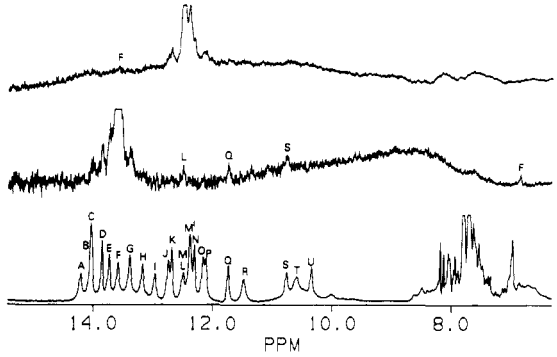


FIGURE 7: 500-MHz NOE difference spectra of resonances F and L recorded at 15 °C. Saturation of resonance F produces NOEs to peaks L, Q, and S, and saturation of L produces a weak, but real, NOE to F.

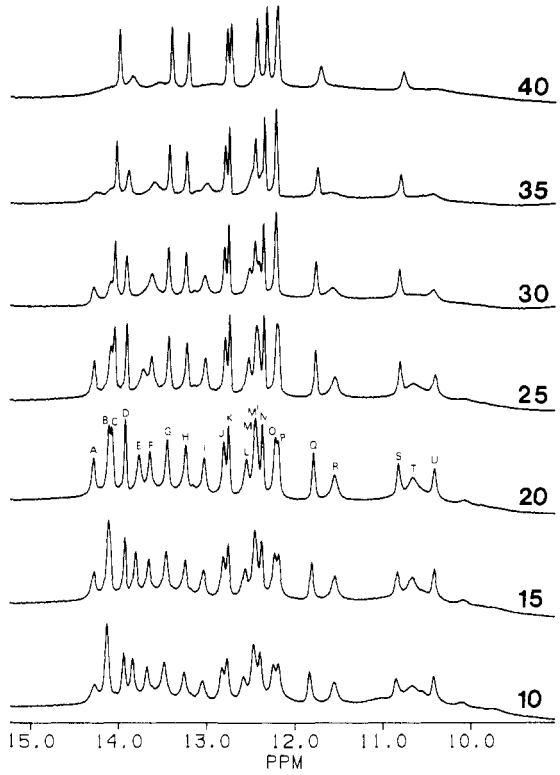


FIGURE 8: 500-MHz imino proton spectrum plotted as a function of temperature in 90% $H_2O$/10% $D_2O$, 20 mM phosphate buffer, pH 7, 0.1 M NaCl, 0.2 mM EDTA, and 0.02% $NaN_3$. The temperature at which each spectrum was recorded is marked in the right-hand margin in degrees celsius.

temperature is increased from 20 to 25 °C, the terminal base pairs and the base pairs closing the hairpin loops of stems I and III (resonances B, E, R, and T) begin to open and exchange with $H_2O$. When the temperature is increased 30 °C, resonance E has completely disappeared, and peaks A, I, R, and T of stem I have broadened significantly. In addition, the terminal base pairs of stem II (resonances F, L, and M′/P) begin to open and exchange with $H_2O$. Increasing the temperature to 35 °C results in a further broadening of these resonances, and finally, at 40 °C only resonances M (the GC base pair of stem I), N and K (the two GC pairs of stem III), and C, O, G, H, Q, and S (the center five base pairs of stem II) remain stable. This uniform "unzipping" from the ends of the individual helical subdomains is in agreement with the assignments of Figure 1 and suggests that there is no cooperativity between the helical stems upon denaturation.

If the RNA tumbles isotropically in solution, we can expect imino proton resonances corresponding to base pairs with long

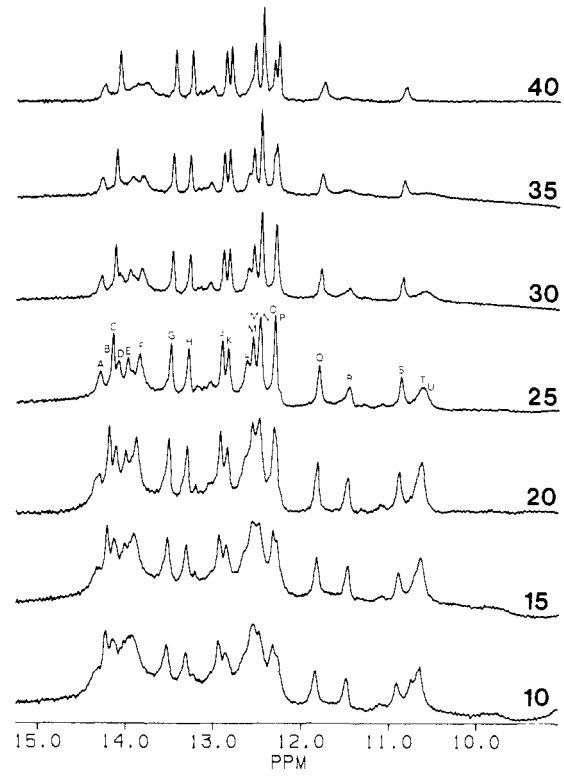


FIGURE 9: 500-MHz imino proton spectrum plotted as a function of temperature in 90% $H_2O$/10% $D_2O$, 20 mM phosphate buffer, pH 7, 0.1 M NaCl, 0.2 mM EDTA, 0.02% $NaN_3$, and 10 mM $MgCl_2$. The temperature at which each spectrum was recorded is marked in the right-hand margin in degrees celsius.

lifetimes on the NMR time scale to have similar line widths. It is clear in Figure 8 that this is not the case. The internal resonances of stem III (D, N, and K) exhibit slightly narrower line widths than do similarly stable base pair resonances associated with stems I and II. Because narrow line widths are indicative of increased molecular motion, this suggests that stem III possesses motion, possibly due to the nick introduced during cleavage, which is independent of the global structure tumbling in solution. Stem II can, in essence, "flap around" independently of the rest of the structure. One would expect that as the temperature increases and the structure denatures, the resonances of stem I and II would approach the line widths of D, N, and K. Comparison of resonances J and K as the temperature increases from 35 to 40 °C shows that this is indeed the case.

Because magnesium ions are required for the cleavage reaction, magnesium chloride was added to the sample with the rationale that it would stabilize tertiary base pairing interactions necessary for cleavage. Figure 9 shows the imino spectrum as a function of temperature in 20 mM $MgCl_2$. Comparing the 20 °C spectrum with that taken in the absence of $MgCl_2$ (Figure 8), it is evident that addition of magnesium ions has not introduced stable tertiary base pairs, as there are no additional resonances in the imino proton spectrum, but this is not to say that addition of $MgCl_2$ has not perturbed the structure. There is general loss of chemical shift dispersion, especially in the regions containing A–F and L–N. Also, resonances B and C as well as resonances T and U have become completely degenerate, suggesting that there is some structural rearrangement upon the addition of magnesium ions.

Addition of magnesium ions has also increased the stability of the helical stems. At 40 °C, resonances A, I, and M of stem I remain, whereas in the absence of magnesium only resonance M remains at this temperature. Also stabilized are the ter-

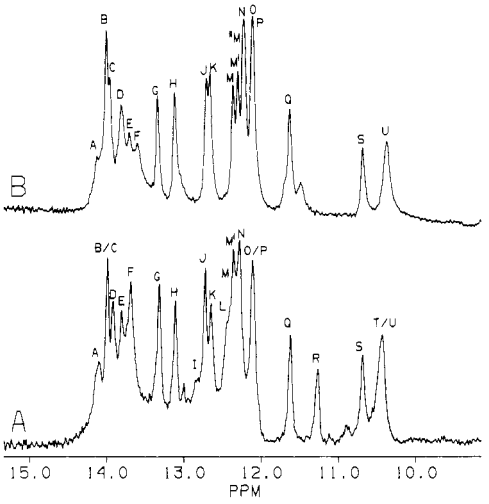


FIGURE 10: (A) 500-MHz imino proton spectrum of cleaved RNA in 90% $H_2O$/10% $D_2O$, 20 mM phosphate buffer, pH 7, 0.1 M NaCl, 0.2 mM EDTA, 0.02% $NaN_3$, and 10 mM $MgCl_2$ recorded at 20 °C. (B) 500-MHz imino proton spectrum of a similar, *uncleaved* RNA in 90% $H_2O$/10% $D_2O$, 20 mM phosphate buffer, pH 7, 0.1 M NaCl, 0.2 mM EDTA, 0.02% $NaN_3$, and 10 mM $MgCl_2$ recorded at 20 °C. This spectrum contains an additional resonance, M″, and is missing resonances R and T due to the replacement of the GU wobble base pair of stem I with a Watson–Crick GC base pair in this RNA sequence.

minal base pairs of stem II (resonances F, L, M′, and P). However, this increased stability is probably due to the increased ionic strength of the solution rather than magnesium ion specific interactions. As the temperature is decreased to 10 °C, the spectrum broadens, resulting in a loss of resolution. The most severe broadening occurs nears the junction of the three helical stems (resonances E, L, and I). This effect is probably associated with $Mg^{2+}$ binding near fast exchange, but without further data, we cannot be more specific. In fact, the cleaved form may no longer have a "good" $Mg^{2+}$ binding site.

It is interesting to note that the resonances of stem III in the presence of magnesium ions do not exhibit narrower line widths than do the resonances of stems I and III as previously discussed. Although resonances N and D are no longer well enough resolved for line-width comparison, it is clear that K, which is still well resolved in 10 mM $MgCl_2$, is not narrower than resonance J. In fact, below 25 °C, resonance K is much broader than J. The addition of magnesium ions to the sample has apparently "tacked down" the once independent stem III, thereby eliminating its independent motion.

To establish the relevancy of the cleaved RNA, its spectrum was compared to that of a similar RNA which contains a mutation causing it to cleave sufficiently slowly that pure, uncleaved RNA could be obtained. The spectra are shown in Figure 10. The sample conditions are given in the figure legend. The sequence of the uncleaved RNA differs slightly from that of the cleaved RNA. In addition to a mutation of one of the conserved residues, the GU wobble base pair of stem I was replaced with a Watson–Crick GC pair. This change results in the loss of resonances R and T, and the introduction of a resonance between 12.5 and 12.0 ppm, labeled M″. The position of this additional resonance is consistent with other RNA species containing a similar stem I sequence (data not shown). Aside from these minor sequence-induced spectral differences, the spectra are very similar, as most of the resonances align exactly. Although further studies of the slowly cleaving form of the RNA are necessary to understand the tertiary structure of the domain, the similarity of the spectra confirms the relevance of these studies as a secondary structural model for the intact hammerhead domain.

## Discussion

The focus of this study was 2-fold. Ultimately our goal is to identify tertiary interactions, in the form of base pairing between conserved nucleotides, which drive the cleavage conformation of a hammerhead-type self-cleaving RNA. However, to achieve this goal, it was necessary to design an RNA that not only cleaved but also exhibited an imino proton spectrum well enough resolved to be completely, unambiguously assigned. This intermediate goal was achieved by replacing two Watson–Crick GC base pairs with GU wobble base pairs. While we have successfully assigned the imino proton spectrum, thereby substantiating, with the exception of two terminal AU base pairs, the hammerhead folding model, we have not reached our final goal. Addition of $MgCl_2$ to the RNA sample did not produce additional imino proton resonances as expected. It is difficult to rationalize the conservation of 13 nucleotides in such a small structure unless they interact in a sequence-specific manner. Therefore, we conclude that cleavage of the RNA results in a subsequent rearrangement of the structure, and this cleaved form does not represent a true three-dimensional cleavage conformation. However, the similarity of the spectrum with that of a comparable, uncleaved RNA proves the relevancy of these studies for the secondary assignments of the hammerhead domain. One could argue that because a folding model was used to help assign the NOE difference spectra, these data represent a circular argument. However, the NOE data are consistent only with the predicted hammerhead folding pattern depicted in Figure 1 (Hutchins et al., 1986; Forster & Symons, 1987; Keese et al., 1987).

The low-field spectrum contains a resonance at ca. 10.5 ppm which was not assigned by NOE difference spectroscopy (labeled U). Due to its chemical shift and lack of NOEs, this resonance was speculated to be that of a U in a hairpin loop region of the molecule. Despite the similarities between this resonance and those of hairpin-looped thymidines of DNA oligomers (Hare & Reid, 1986), further studies are necessary to determine the exact nature of this resonance. We are currently pursuing this goal with the slowly cleaving form of the RNA.

## Acknowledgments

We thank Mr. David Koh for synthesizing the necessary DNA sequences and Dr. Rosalind Kim for the gift of the cloning vector and for sharing her cloning expertise.

## References

Buzayan, J. M., Gerlach, W. L., & Breuning, G. (1986a) *Proc. Natl. Acad. Sci. U.S.A. 83*, 8859–8862.

Buzayan, J. M., Gerlach, W. L., & Breuning, G. (1986b) *Nature 323*, 349–352.

Forster, A. C., & Symons, R. H. (1987) *Cell 49*, 211–220.

Hare, D., & Reid, B. R. (1982a) *Biochemistry 21*, 1835–1842.

Hare, D., & Reid, B. R. (1982b) *Biochemistry 21*, 5129–5135.

Ho, P. S., Fredrick, C. A., Quigley, G. J., van der Marel, G. A., van Boom, J. H., Wang, A. H., & Rich, A. (1985) *EMBO J. 4*, 3617–3623.

Hore, P. J. (1983) *J. Magn. Reson. 55*, 283–300.

Hurd, R. E., & Rein, B. R. (1979) *Biochemistry 18*, 4017–4024.

Hurd, R. E., & Reid, B. R. (1986) *Biochemistry 25*, 5341–5350.

Hutchins, C. J., Rathjen, P. D., Forster, A. C., & Symons, R. H. (1986) *Nucleic Acids Res. 14*, 3627-3640.
Johnston, P. D., & Redfield, A. G. (1978a) *Nucleic Acids Res. 4*, 3599-3615.
Johnston, P. D., & Redfield, A. G. (1978b) *Nucleic Acids Res. 5*, 3913-3927.
Johnston, P. D., & Redfield, A. G. (1979) *Transfer RNA: Structure, Properties, and Recognition*, pp 191-206, Cold Spring Harbor Laboratory, Cold Spring Harbor, NY.
Johnston, P. D., & Redfield, A. G. (1981) *Biochemistry 20*, 1147-1156.
Kearns, D. R. (1976) *Prog. Nucleic Acid Res. Mol Biol. 18*, 91-149.
Kearns, D. R. (1977) *Annu. Rev. Biophys. Bioeng. 6*, 477-523.
Kearns, D. R., & Shulman, R. G. (1974) *Acc. Chem. Res 7*, 33-39.
Keese, P., & Symons, R. H. (1987) in *Viroids and Viroid-like Pathogens* (Semancik, J. S., Ed.) pp 1-47, CRC Press, Boca Raton, FL.
Kneale, G., Brown, T., Kennard, O., & Rabinovich, D. (1985) *J. Mol. Biol. 186*, 805-814.
Leroy, J.-L., Broseta, D., & Guéron, M. (1985) *J. Mol. Biol. 184*, 165-178.
Lowary, P., Sampson, J., Milligan, J., Groebe, D., & Uhlenbeck, O. C. (1987) *NATO ASI Ser. 110*, 69-76.
Maniatis, T., Fritsch, E. F., & Sambrook, J. (1982) *Molecular Cloning: A Laboratory Manual*, Cold Spring Harbor Laboratory, Cold Spring Harbor, NY.
Prody, B. A., Bakos, J. T., Buzayan, J. M., Schneider, I. R., & Breuning, G. (1986) *Science 231*, 1577-1580.
Reid, B. R. (1981) *Annu. Rev. Biochem. 50*, 969-996.
Reid, B. R. & Hurd, R. E. (1977) *Acc. Chem. Res. 10*, 396-402.
Reid, B. R., & Hurd, R. E. (1979) *Biochemistry 18*, 3996.
Reid, B. R., Ribeiro, N. S., Gould, G., Robillard, G., Hilbers, C. W., & Shulman, R. G. (1975) *Proc. Natl. Acad. U.S.A. 72*, 2049-2055.
Reid, B. R., Ribeiro, N. S., McCollum, L., Abatte, J., & Hurd, R. E. (1977) *Biochemistry 16*, 2086-2094.
Roy, S., & Redfield, A. G. (1981) *Nucleic Acids Res. 9*, 7073-7083.
Sanchez, V., Redfield, A. G., Johnston, P. D., & Tropp, J. (1980) *Proc. Natl. Acad. Sci. U.S.A. 77*, 5659-5662.
Schimmel, P. R., & Redfield, A. G. (1980) *Annu. Rev. Biophys. Bioeng. 9*, 181-221.

# Kinetic Isotope Effect Studies on Milk Xanthine Oxidase and on Chicken Liver Xanthine Dehydrogenase†

Susan C. D'Ardenne and Dale E. Edmondson*
*Department of Biochemistry, Emory University School of Medicine, Atlanta, Georgia 30322*
*Received March 7, 1990; Revised Manuscript Received June 26, 1990*

ABSTRACT: The effect of isotopic substitution of the 8-H of xanthine (with $^2H$ and $^3H$) on the rate of oxidation by bovine xanthine oxidase and by chicken xanthine dehydrogenase has been measured. $V/K$ isotope effects were determined from competition experiments. No difference in $^{H/T}(V/K)$ values was observed between xanthine oxidase (3.59 ± 0.1) and xanthine dehydrogenase (3.60 ± 0.09). Xanthine dehydrogenase exhibited a larger $^{T/D}(V/K)$ value (0.616 ± 0.028) than that observed for xanthine oxidase (0.551 ± 0.016). Observed $^{H/T}(V/K)$ values for either enzyme are less than those $^{H/T}(V/K)$ values calculated with $^{D/T}(V/K)$ data. These discrepancies are suggested to arise from the presence of a rate-limiting step(s) prior to the irreversible C-H bond cleavage step in the mechanistic pathways of both enzymes. These kinetic complexities preclude examination of whether tunneling contributes to the reaction coordinate for the H-transfer step in each enzyme. No observable exchange of tritium with solvent is observed during the anaerobic incubation of [8-$^3H$]xanthine with either enzyme, which suggests the reverse commitment to catalysis ($C_r$) is essentially zero. With the assumption of adherence to reduced mass relationships, the intrinsic deuterium isotope effect ($^Dk$) for xanthine oxidation is calculated to be 7.4 ± 0.7 for xanthine oxidase and 4.2 ± 0.2 for xanthine dehydrogenase. By use of these values and steady-state kinetic data, the *minimal* rate for the hydrogen-transfer step is calculated to be ~75-fold faster than $k_{cat}$ for xanthine oxidase and ~10-fold faster than $k_{cat}$ for xanthine dehydrogenase. This calculated rate is consistent with data obtained by rapid-quench experiments with XO. A stoichiometry of 1.0 ± 0.3 mol of uric acid/mol of functional enzyme is formed within the mixing time of the instrument (5-10 ms). The kinetic isotope effect data also permitted the calculation of the $K_d$ values [Klinman, J. P., & Matthews, R. G. (1985) *J. Am. Chem. Soc. 107*, 1058-1060] for substrate dissociation, including all reversible steps prior to C-H bond cleavage. Values calculated for each enzyme ($K_d$ = 120 μM) were found to be identical within experimental uncertainty.

In spite of a considerable number of pre-steady-state kinetic studies (Olson et al., 1974a,b; Brugeura et al., 1988; Coughlan & Rajagopalan, 1980; Rajagopalan & Handler, 1967; Edmondson et al., 1973) there are still a large number of questions unanswered regarding the initial reductive step in the catalytic mechanism of xanthine oxidase (XO)[1] or of xanthine dehydrogenase (XDH). The involvement of the molybdenum center as the initial site of entry of reducing

† This work was supported by grants from the National Science Foundation (DMB-8616952) and from the National Institutes of Health (GM-29433).

[1] Abbreviations: XO, xanthine oxidase; XDH, xanthine dehydrogenase; $NAD^+$, nicotinamide adenine dinucleotide, oxidized; HPLC, high-pressure liquid chromatography; ESR, electron spin resonance.

0006-2960/90/0429-9046$02.50/0 